AIAA JOURNAL
Vol. 60, No. 7, July 2022

Experimental Investigation of Abrupt Change in a Scramjet with Variable Mach-Number Flow

Zhenjie Wu,* Qifan Zhang,† Xu Zhang,‡ Weihang Luo,§ Zhanbiao Gao,¶ and Lianjie Yue**
State Key Laboratory of High Temperature Gas Dynamics, Institute of Mechanics, Chinese Academy of Sciences, 100190 Beijing, China

https://doi.org/10.2514/1.J061287

To study an abrupt phenomenon of a scramjet in the Mach-number variation process, a scramjet model was tested in the simulated acceleration and deceleration conditions between the flight Mach numbers of 5.0 and 6.0. The results showed that once the flame stabilization changes, the pressure and thrust will meet the abrupt change simultaneously, while three typical flame stabilization and two types of transformation processes were found. One is the switching between the jet-wake flame and the cavity shear-layer flame directly, accompanied by one abrupt change. The other is the switching of the first two flame stabilizations, combined with the cavity shear-layer/recirculation flame, accompanied by two abrupt changes. The reduction in the range of the equivalence ratio and the process of increasing the Mach number will promote the appearance of the second type with two abrupt changes, and the process of increasing equivalence ratio and decreasing Mach number makes the first type with only one abrupt change more likely to occur. In other words, the characteristics of the abrupt change during the flame stabilization transition process are determined by the combined effect of the changing paths of the incoming flow condition and the equivalence ratio. The actual process of Mach- number variation has an obvious historical effect on the flame stabilization transition.

I. Introduction

IN RECENT years, near-space vehicles have become the research focus in major aerospace countries. Scramjet is an ideal thruster for near-space vehicles. The air-breathing cycle can achieve a high specific impulse without carrying an oxidizer, which has obvious advantages over rocket engines. However, due to the high-velocity airflow and short residence time in the combustor of the engine, flame stability has always been a key issue in scramjet engine research [1–4].

In early experimental studies, measurement means were scarce, and combustion test data were generally limited to pressure [5–8]. Then the one-dimensional Mach number along the range was determined, which is an inversion result from the pressure. Based on such analysis means, the engine was classified into the two operating modes of supersonic combustion mode or subsonic combustion mode according to the Mach-number distribution. In the past few decades, some advanced measurement technologies have gradually been applied to scramjet ground tests. Researchers can directly observe the flowfield structure and flame pattern, which is helpful to classify the types of flame stabilization modes. Therefore, more and more scholars began to study the flame in the combustor [9–11]. According to the results of the direct-connect experiment, Driscoll et al. [12,13] found that there are two distinct flame stabilization locations in the combustor for different total temperatures of the incoming flow: one is anchored at the leading edge of the cavity by heat release in the cavity shear layer, and the other is stabilized a short distance downstream of the fuel-injection jet in the jet wake. Furthermore, Rasmussen et al. [14,15] found two characteristics of cavity-stabilized flames. One is the flame stability in the shear layer, and the other is the flame stability in the cavity. These locations would vary, as the equivalence ratio of fuel and location of fuel injectors are varied [16]. Experimental observations and numerical simulation were carried out to study the flame stabilization mechanism in a supersonic combustor by Sun et al. [17]. Different cavity configurations will lead to different flame stabilization modes [18]. According to the flame structure and location of the direct-connect experiment, Wang et al. [19,20] indicated that there are three flame modes: cavity assisted jet-wake stabilized flame, cavity shear-layer stabilized flame, and combined cavity shear-layer/recirculation stabilized flame. The combustion intensity of the jet-wake stabilized flame is stronger than the combustion intensity of the combined cavity shear-layer/recirculation stabilized flame, and both are stronger than the combustion intensity of the cavity shear-layer stabilized flame. Different flame stabilization modes have different characteristics of the pressure distribution. A typical pressure distribution along the way under different flame stabilization modes was given by Yuan et al. [21]. The start of the pressure rise is within the isolator, which means that the flame stabilization mode is jet-wake stabilized combustion. When the flame stabilization mode is combined with cavity shear-layer/recirculation stabilized combustion, the maximum pressure rise is at the rear edge or downstream of the cavity. If the maximum pressure rise is relatively small and inside the cavity, the flame stabilization mode is a cavity shear-layer stabilized flame.

Different pressure distribution characteristics in different flame stabilization modes mean different thrust performances. Therefore, the transition of the flame stabilization mode may cause abrupt changes in wall pressure and thrust. Abrupt changes in pressure and engine thrust are detrimental to vehicle control, and many studies have been carried out on these. Therefore, experiments with different equivalence ratios under the conditions of constant Mach flow supplied by the direct-connect supersonic combustor facility were carried out. The equivalence ratio changes only a certain amount near a certain quantitative ratio, and the variation in the pressure will meet an abrupt change [22–24]. The preceding experiments are achieved by adjusting the equivalence ratio at discrete points to achieve the change in the equivalence ratio. To further study the dynamic process of pressure mutation, researchers conducted many experiments to continuously increase the equivalence ratio. Xiao et al. [25] found that an increase in the equivalence ratio would result in an abrupt change in pressure. Zhang et al. [26] used the strut configuration to study the abrupt changes in wall pressure and thrust under the conditions of Ma 5.0 and a variable equivalence ratio. A Laval nozzle of alterable throat area was developed

Received 17 September 2021; revision received 16 February 2022; accepted for publication 30 April 2022; published online 30 May 2022.

*Ph.D. Candidate; also School of Engineering Sciences, University of Chinese Academy of Sciences, 100049 Beijing, China.
†Research Assistant; zhangqifan@imech.ac.cn (Corresponding Author).
‡Postdoctoral Researcher.
§Junior Engineer.
¶Engineer.
**Professor; also School of Engineering Sciences, University of Chinese Academy of Sciences, 100049 Beijing, China.

by Zhang et al. [27] to change the incoming flow Mach number at the entrance to the isolator, and different pressure- distribution variations were obtained by changing the incoming flow Mach number and total pressure at a constant equivalence ratio. Kouchi et al. [28] conducted a numerical simulation of a compression scramjet engine under Mach 6 flight conditions and captured the abrupt change in thrust. Turner and Smart [29] found that certain engine configurations will have an abrupt change in the thrust coefficient. In the preceding research, abrupt changes in pressure and thrust were believed to be caused by conversion of the combustion mode. Through three-dimensional numerical calculations, X. Zhang [30,31] proved that the root cause of the abrupt changes was the flame stabilization mode transition.

In previous research, the study on abrupt changes in pressure and thrust used mainly a direct-connect scramjet model and focused on the effect of the equivalence ratio at a fixed Mach number. Due to the historical effect of combustion, the variation in the incoming Mach number will also cause a mode transition [27]. The variation in the Mach number will inevitably be coupled with the equivalence ratio, which may bring new changes to the aforementioned abrupt-change-phenomenon/steady-flame mode transition process. Currently, due to the limitation of experimental equipment and the large amount of calculation in the variation process of the Mach number, there are few relevant studies in this area. With the development of the scramjet, the cognitive demand in this area has become more urgent. The thrust of the engine is jointly determined by the inlet, combustor, and nozzle [32]. The lack of inlets and nozzles in the direct-connected scramjet model leads to an inaccurate evaluation of thrust during experiments. Therefore, the current paper experimentally investigates the influence of variable Mach flow conditions on the abrupt change in pressure and thrust of the scramjet model with cavity configuration, by the variable-Mach-number hypersonic-propulsion test facility.

II. Experimental Approach

A. Variable-Mach-Number Hypersonic-Propulsion Test Facility

The experiments were performed at the variable-Mach-number hypersonic-propulsion test facility of the Institute of Mechanics, Chinese Academy of Sciences. This facility shown in Fig. 1 can simulate the inflow conditions of a maximum total temperature of 1950 K and a total pressure of 6 MPa within an effective operating time of 100 s. The outlet size of the wind-tunnel nozzle is 330 × 330 mm, providing nominal freestream Mach numbers from 4.5 to 6.5, although the actual range can be larger. The specific operating range of the wind tunnel is shown in Table 1. The variable-Mach hypersonic-propulsion test facility consists mainly of four parts: heater, nozzle, test section, and ejector. The heater and the nozzle are the core parts of the facility and have an accurate adjustment capacity to achieve the Mach number variation. The specific nozzle is a rectangular variable-Mach-number nozzle, and the nozzle outlet size is fixed. During the running time, the lower wall of the nozzle rotates around the lower edge of the nozzle outlet to change the nozzle throat area and implement the continuous variation of the Mach number. In addition, to obtain high total temperature and total pressure, hydrogen is burned with air in the heater while oxygen is supplied to maintain a 21% mole fraction of oxygen. The stagnation

Table 1 Typical calibration result of the continuously variable-Mach-number hypersonic- propulsion test facility

Nominal Mach number variation range	4.5–6.5
Flight altitude range	20–30 km
Maximum total pressure	6.0 MPa
Maximum total temperature	1950 K
Dimensions of nozzle outlet	330 mm × 330 mm
Maximum mass flow rate	20 kg/s
Maximum running time	100 s

parameters of the incoming flow can be varied by adjusting the mass flow rates of hydrogen, oxygen, and air. The valve adjustment system is introduced to ensure that the mass flow rate of each component in real time matches the dynamic variation of the Mach number, the total pressure, and the total temperature to perfectly simulate the real-time variation process of the scramjet in actual flight.

Considering the complexity of variable–Mach-number engine tests, the following is a brief description of the experimental procedures and the time sequence in this paper in conjunction with Fig. 2. At the start of the test, the ejector will be the first to turn on to establish the vacuum condition required for the nozzle to start. Once the vacuum is stabilized, the heater will operate to create a steady high-enthalpy incoming flow and establish the initial wind-tunnel flowfield from time t_1. Subsequently, pilot hydrogen is injected into the combustor and ignited by spark plugs. The easy ignition and high calorific value of hydrogen is used as a high-energy ignition source to ignite the subsequent injection of ethylene fuel. When stable combustion of ethylene is obtained, the pilot hydrogen injection will be turned off to ensure that the subsequent period is a pure ethylene burning phase for the effective test time. During this period, the wind tunnel will accomplish the process of variable-Mach-number adjustment, and ethylene fuel injection will also be adjusted in real time as the incoming flow changes. The entire pure ethylene test time is approximately 4.7 s, starting from $t_4 = 15.0$ s and ending at $t_7 = 19.7$ s. The Mach number varies linearly from $t_5 = 15.6$ s to $t_6 = 18.8$ s.

B. Scramjet Model and Test Conditions

The scramjet model studied in this paper has a total length of approximately 2.0 m, including the inlet, isolator, combustor, and

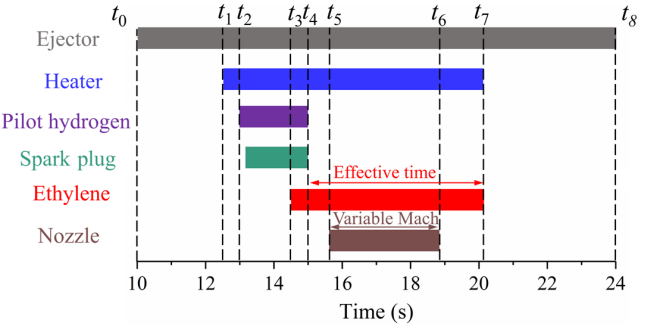

Fig. 2 Brief description of the experimental steps and the time sequence.

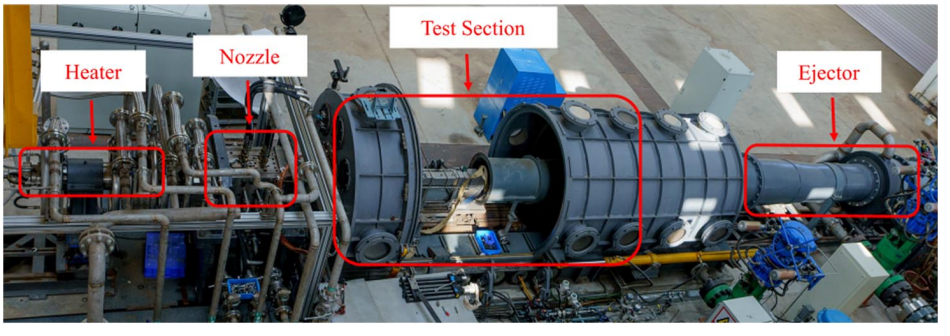

Fig. 1 The variable Mach hypersonic-propulsion test facility.

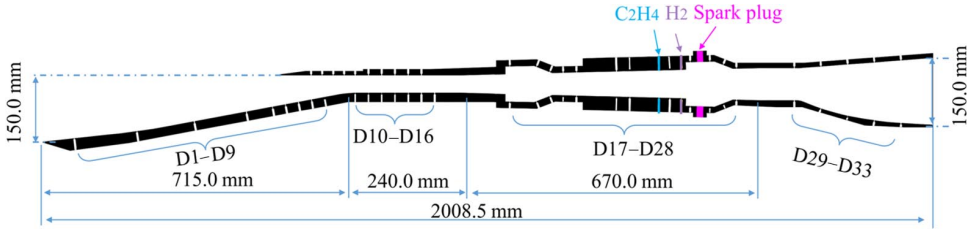

Fig. 3 Geometric parameters of the scramjet model.

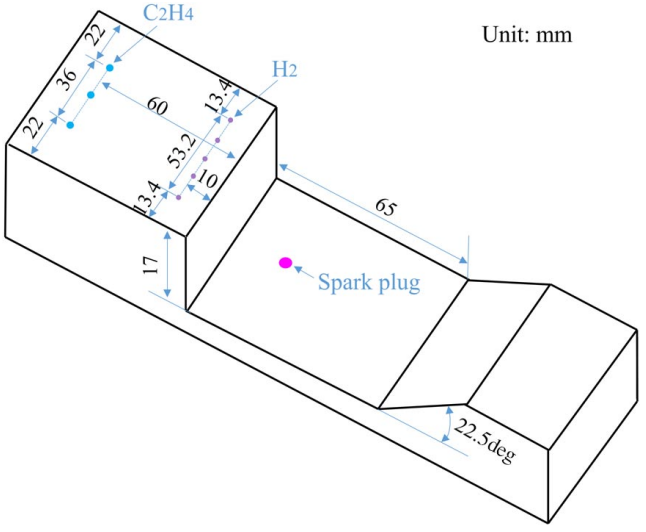

Fig. 4 Schematic of the cavity.

nozzle. The structure and dimensions are shown in Fig. 3. The inlet adopts a two-stage compression design of a 6 deg oblique shock wave and a 4.5 deg isentropic wave, with a capture area of 150×80 mm^2 and a length of 715 mm. The inlet throat is 40 mm high, and an isolator that is 240 mm long directly follows the throat. The combustor behind the isolator has a constant-width expansion structure with an expansion angle of 2.8 deg. The total length and exit height of the combustor are 670 and 72.75 mm, respectively. Behind the combustor is the nozzle with a length of 396 mm. The front section of the nozzle is an equal straight section with a length of 80 mm that then expands to 150 mm in exit height, which is the same as the capture height of the inlet. The combustor adopts a double-row four-cavity structure, and the cavities on the upper and lower walls are designed symmetrically in the flow direction. The positions of the cavities relative to the combustor entrance are 100 and 506 mm. The specific structure of a single cavity and the size of the injection holes are shown in Fig. 4. The depth and length of the cavity and the angle of the trailing edge of the cavity are 17 mm, 65 mm, and 22.5 deg, respectively. The ethylene injection holes and the hydrogen guiding injection holes are located 60 and 10 mm upstream of the cavity, respectively, and the igniter is located at the bottom of the cavity. Three injectors of ethylene are distributed with an equal spanwise-distance of 18 mm in the upper and lower walls of the combustor. Each injector of ethylene has circular cross sections with the same diameter of 2.0 mm. There were five 0.8- mm-diameter porthole injectors of hydrogen with an equal spanwise-distance of 13.3 mm on each side of the upper and lower walls of the combustor.

To improve the starting ability of the wind tunnel and maintain the uniformity of the engine inlet flowfield, the inlet of the scramjet model was designed as a truncated inlet. Specifically, this paper removes the first-stage 6 deg compression from the previously designed three-stage compression inlet and retains only the subsequent two-stage compression. Then, the internal flowpath is turned to the level of the first-stage compression surface, to obtain the preceding two-stage-compression truncated inlet. Corresponding to the truncated inlet, the incoming flow parameters of the wind tunnel will also be adjusted to the parameters of the flight incoming flow conditions compressed by 6.4 deg, considering the additional effect of the boundary layer. For the actual flight simulation in this paper, the actual wind-tunnel inflow conditions of the airflow parameters after simulated flight conditions are virtually compressed through the inlet at 6.4 deg under the conditions of Ma 5.0 acceleration to Ma 6.0. Therefore, corresponding to the process of wind-tunnel airflow acceleration from Ma 4.4 to Ma 5.1, the specific parameters are shown in Table 2. In the following description and analysis, to avoid confusion between the simulated flight Mach number and the actual test Mach number, the flight Mach numbers will be used to characterize the test conditions.

For the same purpose, to reduce the frontal area of the engine, the nozzle of the scramjet model is also truncated. In addition, a rectangular nozzle extension cover with a half-open structure is installed at the nozzle outlet in Fig. 5 to extend the nozzle uniform area to cover the engine inlet. Furthermore, two oblique baffles are added on both sides of the inlet forebody to avoid the impact of the three-dimensional flow and obtain the two-dimensional flowfield for the inlet.

C. Measurement Facilities

Because the test in this article involves multiple variable parameter systems, both the test facility and the scramjet model are equipped with multiple test systems. The following will be introduced one by one. The first is the system of the facility. To monitor the variations in the incoming flow, the pressure sensor UNIK 5000 by General Electric with a pressure measurement accuracy of 0.1% full scale (herein abbreviated as FS) was installed upstream of the nozzle. The FS of the pressure sensor is 20 MPa. At the same time, a set of displacement sensors is installed at the throat of the variable-Mach-number nozzle to measure the geometric state of this nozzle. Ethylene fuel undergoes dynamic adjustment of the equivalent ratio through an electric pressure reducing valve, and its flow is obtained with a differential-pressure orifice flowmeter. The differential-pressure transmitter has a range of 0.4–40 kPa and an accuracy of 0.1% FS, which can ensure high-precision flow measurement.

For the scramjet model, the wall pressure measurement and the direct thrust measurement are used mainly to obtain the internal flowfield and performance of the engine. Specifically, as shown in Fig. 2, 60 pressure measuring points are arranged on the upper and lower walls of the scramjet model. There were 27 (U1–U27) pressure

Table 2 Correspondence between flight conditions and variable Mach hypersonic-propulsion- test-facility flow conditions

Flight condition				Test condition			
Mach number	Static pressure, kPa	Total temperature, K	Total pressure, MPa	Mach number	Static pressure, kPa	Total temperature, K	Total pressure, MPa
6.0	2.11	1513	3.88	5.1	5.06	1513	3.63
5.0	2.88	1185	1.66	4.4	6.07	1185	1.59

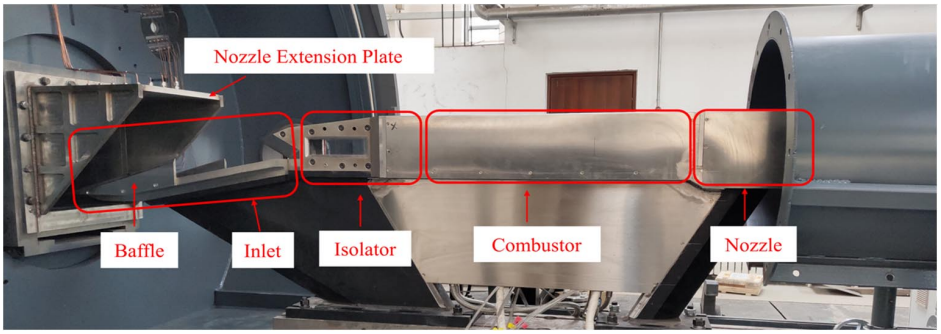

Fig. 5 Scramjet model mounted on the test section of the variable Mach hypersonic-propulsion test facility.

measuring points on the upper wall, and 33 (D1–D33) pressure measuring points on the lower wall. Wall pressure is measured with the DTC Initium ESP-32HD electronic pressure scanning module with 0.25% accuracy and a 652 Hz sampling frequency. Considering the lower pressure of the inlet and nozzle than the combustor, a range of 45 psi electronic pressure scanning modules is used in the inlet and nozzle, whereas a range of 100 psi electronic pressure scanning modules is used in the combustor. To obtain the dynamic variation process of the engine thrust in the variation process, the 13-CYZH-02A cassette strain gauge balance of the AVIC Aerodynamics Research Institute is placed under the scramjet model. The balance can measure three-coordinate forces, and the specific axial force range of the balance is ±4000 N with a standard measurement uncertainty of 0.30% FS. The balance signal was acquired by the DH5939E high-frequency signal acquisition system of Donghua Testing Technology Co., Ltd., with a sampling frequency of 1 kHz.

In addition to the preceding measuring methods, two pressure sensors are installed on hydrogen and ethylene fuel-supply pipes to monitor fuel-injection pressures and timing. The two sensors were recorded at 100 Hz by the Pacific Instruments series 6000 data acquisition system. Moreover, all experimental data acquisitions are triggered by the same transistor—transistor logic signal source to ensure recording-time consistency of these data.

III. Results and Discussion

The variable-Mach hypersonic-propulsion test facility provides flow simulations with flight Mach numbers varying from 5.0 to 6.0 and vice versa. To reduce the number of variables, only one place in the second cavity is selected for fuel injection. First, test A1 is carried out to study the abrupt change in thrust during acceleration. Then, the influence of equivalence ratio variation on the thrust during acceleration is present in test A2. Finally, the comparison of thrust variation during acceleration and deceleration is investigated by tests A3 and A4. In the deceleration test A5, the equivalence ratio is kept basically unchanged to explore the effect of only the incoming flow change on the transition of the flame stabilization mode.

A. Abrupt Change in Thrust During Acceleration

To obtain the abrupt thrust phenomenon, the experiments are designed as jet-wake stabilized combustion at a low Mach number, and cavity shear-layer stabilized combustion at a high Mach number [33]. The acceleration flight condition and equivalence ratios are shown in test A1. Corresponding to the acceleration period of 3.2 s from 15.6 s to 18.8 s, the equivalence ratio varies from 0.53 to 0.16.

Figure 6 exhibits the corresponding distributions of the time-averaged surface pressure and the uncertainty of the scramjet model at different times in the acceleration process. To reduce the influence of data fluctuation on the experimental results, the integral time is chosen as 0.05 s to obtain the averaged values from the pressure–time histories, and the pressures are normalized by the freestream static pressure of the corresponding moment. The uncertainty of the data measured in the experiment is calculated using the Bessel formula. Because the pressure ratio is an indirect measurement parameter, the uncertainty is calculated according to the indirect measurement uncertainty formula.

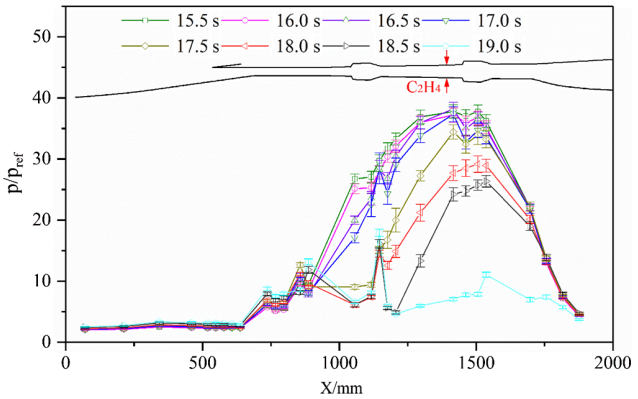

Fig. 6 Pressure ratio distributions along the lower wall at different times of test A1.

First, let us take a look at 15.5 s; the flight condition is Ma 5.0. The inlet-ramp-side surface pressures increase step by step along the streamwise direction due to the compression effect of the ramp shocks. In response to the reflections of the shock waves and the expansion waves, the surface pressure distribution of the isolator undulates along the flow direction in the front half of the isolator. A pressure rise can be found at $X = 800$ mm in the latter half of the isolator, corresponding to the high equivalence ratio of fuel. The pressure along the way rises continuously in the combustor and reaches the highest value in the second cavity, where the fuel is injected. Then, the air flows through the rear edge of the cavity and expands with acceleration. Due to the sustained action of the expansion section and the downstream nozzle, the pressure continuously decreases. With increasing time, the intensity of the inlet wave system becomes stronger as the Mach number of incoming flows increases, which leads to a continuous increase in the pressure distribution along the inlet. However, the equivalence ratio continuously decreases, so the starting point of the high-pressure zone in the combustor keeps moving backward, and the maximum pressure near the cavity also gradually decreases. The pressure in the combustion zone dropped significantly during the time period from 18.5 to 19.0 s, and the maximum pressure ratio in the downstream cavity area was dramatically reduced from 25 to 9. According to the pressure distribution characteristics of typical flame stabilization modes presented in the referenced article of Yuan et al. [21], the flame stabilization mode can be judged to be jet-wake stabilized combustion before 18.5 s. As the time increases to 19.0 s, the flame stabilization mode transitions from jet-wake stabilized combustion to cavity shear-layer stabilized combustion.

Figure 6 shows the abrupt change in the surface pressure distributions of the scramjet model during the acceleration process, which will directly affect the thrust performance of the scramjet. With the help of the cassette strain gauge balance, the joint forces of the scramjet model can be measured. However, the joint forces include the external resistance and internal resistance in addition to the thrust. Furthermore, these forces will change with the variation of the incoming flow. To obtain the evolution characteristics of the engine

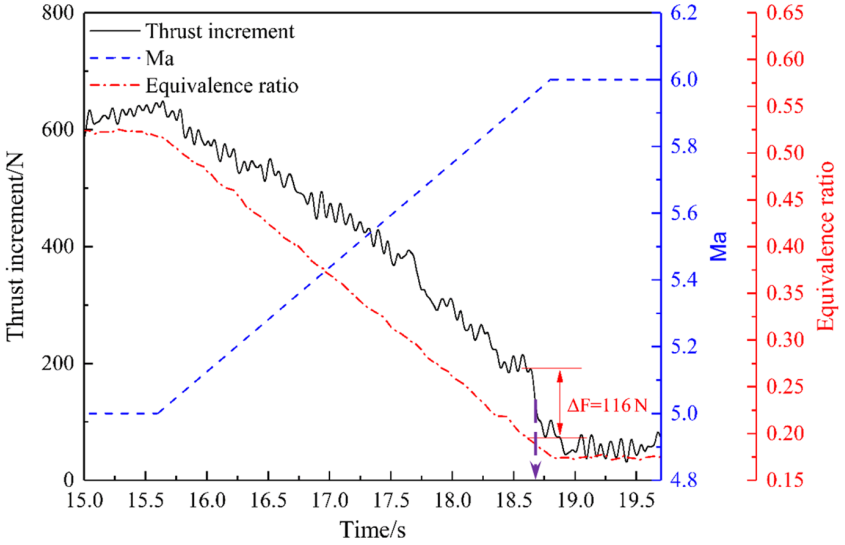

Fig. 7 Thrust increment and equivalence ratio vs time of test A1.

thrust, we need to remove such interference factors by carrying out the no-fuel test corresponding to test A1. By deducting the joint–force–time history of the no-fuel injection test, the thrust increment time history generated by combustion under the A1 operating condition can be obtained in Fig. 7. To better obtain the nonlinear characteristic of the thrust, the thrust data are subjected to 10-Hz low-pass filter processing to remove the fluctuation disturbance. The thrust increment reaches the maximum value of 650 N between 15.0 and 15.6 s. The thrust increment associated with the acceleration process starts to decrease. An abrupt change in the thrust increment can be noted at approximately 18.7 s, and the magnitude of the thrust increment decrease is 116 N, which is equivalent to 17.8% of the maximum value of the thrust increment. The time of 18.7 s is included in the flame stabilization mode transition process in Fig. 6. Therefore, the relationship between the abrupt change in thrust and the abrupt change in pressure will be further analyzed subsequently by analyzing the pressure–time history of the measuring points near the second cavity.

Because the fuel is injected upstream of the second cavity, the pressure data of the measuring points around the second cavity are more representative of the combustion characteristics. The pressure–time histories of measuring points D24, D26, and D28 located at the cowl side are shown in Fig. 8. The D24 measuring point is immediately upstream of the second cavity. The D26 survey point is located in the second cavity, and the D28 survey point is located immediately downstream of the second cavity. Compared to the thrust data in Fig. 7, a similar abrupt change in the time of 18.7 s can be found in the pressure–time histories of these three measuring points, which indicates that an abrupt reduction in the combustion intensity occurs. Abrupt changes in the pressure and thrust apparently occur at the same time, so it can be presumed that the abrupt change in thrust is caused by the abrupt change in pressure. Furthermore, the entire flame stabilization mode transition process is very fast, as shown in Figs. 7 and 8. In other words, the abrupt changes in pressure and thrust are the results of flame stabilization mode transitions from jet-wake stabilized combustion to cavity shear-layer stabilized combustion, which is in agreement with the simulation results of Zhang et al. [30].

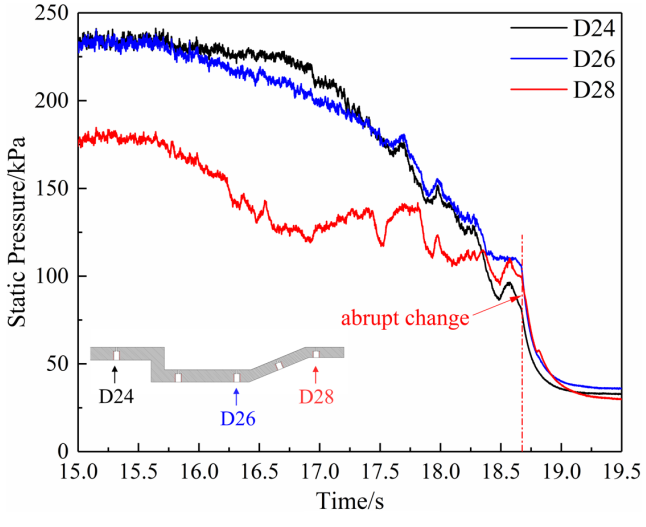

Fig. 8 Pressure of the measuring point near the cavity vs time of test A1.

B. Effect of the Equivalence Ratio Variation

To determine the influence of the equivalence ratio variation on the abrupt change in thrust, test A2 was carried out. Compared to test A1, a smaller amplitude of equivalence ratio variation is adjusted in test A2, varying from 0.30 to 0.15. Figure 9 presents the thrust increment versus time during the experimental process of test A2. Two abrupt changes in the thrust increment occurred at approximately 18.55 and 18.75 s in test A2, which is different from one abrupt change in the thrust increment of test A1. The first change was at 18.55 s with an abrupt change amplitude of 90 N, and the second change was at 18.75 s with an abrupt change amplitude of 63 N. Obviously, the amplitude of the first abrupt change is greater than the amplitude of the second change. Using the previous analytical methods, the wall pressure data of test A2 will be presented to explore the mechanism of the two abrupt changes in the thrust.

First, the pressure–time variation curve of the measuring point near the downstream cavity is given in Fig. 10. The static pressures of D24, D26, and D28 start to rapidly decrease at approximately 18.5 s, which indicates a sudden decrease in the combustion intensity. However, the pressure at measuring point D28 did not show a continuous decrease like the other two measuring points did, but a pressure plateau of 65 kPa with a duration of approximately 0.2 s occurred near 18.75 s. Then, there was the second sudden drop in the pressure at D28, and the pressure value after the sudden drop was basically equal to the pressure at the D24 and D26 measuring points. From the time viewpoint, the time of the second abrupt change in pressure at the D28 measuring point is consistent with the time of the second abrupt change in thrust in Fig. 10. That is to say, there is a certain correlation between the two abrupt changes. Then, the distributions of the pressure ratio on the ramp-side of the scramjet at different times are obtained in Fig. 11. The first abrupt change in pressure occurred between 18.5 and 18.7 s. The pressure in the downstream cavity area dropped significantly as a whole. The high-pressure region moves from the upstream of the cavity to the rear edge of the

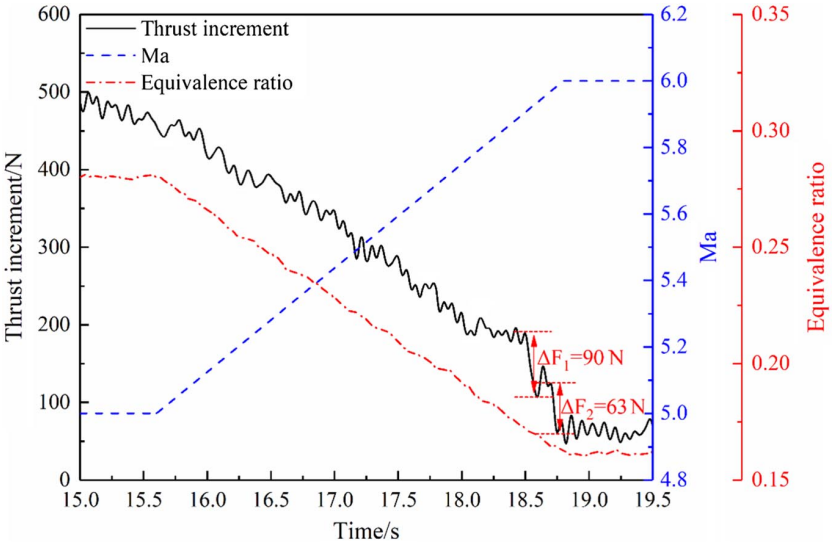

Fig. 9 Thrust increment and equivalence ratio vs time of test A2.

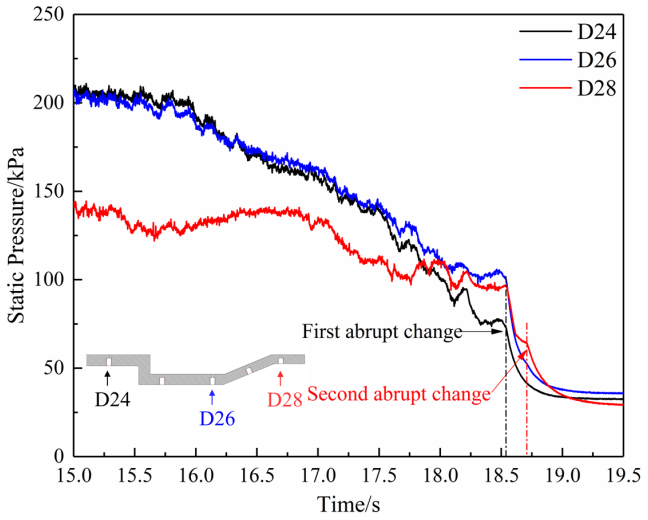

Fig. 10 Pressure of the measuring point near the cavity vs time of test A2.

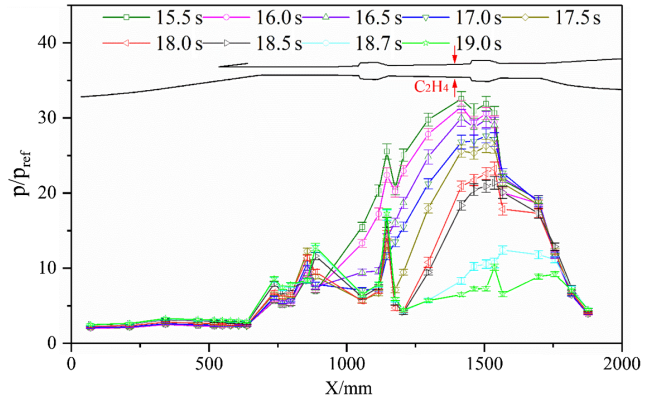

Fig. 11 Pressure ratio distributions along the lower wall at different times of test A2.

cavity and downstream of the cavity. According to the analysis of the pressure distribution characteristics of different flame stabilization modes in the literature [21], the flame stabilization mode transitions from jet-wake stabilized combustion to combined cavity shear-layer/recirculation stabilized combustion. The second abrupt change in pressure occurred between 18.7 and 19.0 s. During this period, the high-pressure region moves from the downstream of the cavity to the cavity center, which indicates that the flame stabilization mode transitions from combined cavity shear-layer/recirculation stabilized combustion to cavity shear-layer stabilized combustion. The two transitions of the flame stabilization mode are accompanied by two abrupt changes in thrust and pressure in test A2. In other words, the times of the abrupt changes in the pressure and the thrust are decided by the times of the flame stabilization mode transition during the test.

Based on the results of test A2, the accelerating process will reduce the combustion intensity, similar to test A1. The target equivalent ratios of tests A1 and A2 are almost the same, but the initial equivalent ratio of test A1 is significantly higher than that of test A2. Due to the positive effect of the higher equivalent on the combustion intensity, the combustion flame mode transition timing is delayed by approximately 0.15 s in test A1 compared to test A2, and the transition Mach number increases from 5.90 to 5.96. Therefore, the differences in the incoming flow conditions and the fuel-supply status at the mode transition moment will directly affect the magnitude of the abrupt changes in the pressure and thrust, and even the times of the abrupt changes.

C. Abrupt Change in Thrust During Deceleration

As mentioned in the preceding discussions, the acceleration process is accompanied by abrupt changes in pressure and thrust. In consideration of the coexistence of the acceleration and deceleration processes under actual flight conditions, deceleration tests were also carried out in this paper. As shown in Table 3, the corresponding values of the Mach number variation range and equivalence ratio are almost the same in the corresponding deceleration experiments for comparisons, as tests A3 and A4 correspond to tests A1 and A2, respectively.

Figure 12 exhibits the thrust increment vs Mach number for acceleration test A1 and deceleration test A3. To improve the degree of comparability, the thrust increment data of the two tests are both presented on the same x axis with increasing Mach number. There is an abrupt change in thrust in both the acceleration and deceleration tests. However, the magnitude of the abrupt change in thrust and the corresponding Mach number observed while the abrupt change emerges are different between the acceleration and deceleration tests. The abrupt change in thrust occurs at Mach 5.96 during the accel-

Table 3 Flight conditions and equivalence ratios

Test case	Flight condition	Equivalence ratio
A1	Ma 5.0–6.0	0.53–0.16
A2	Ma 5.0–6.0	0.30–0.15
A3	Ma 6.0–5.0	0.15–0.54
A4	Ma 6.0–5.0	0.14–0.29
A5	Ma 6.0–5.0	0.11–0.12

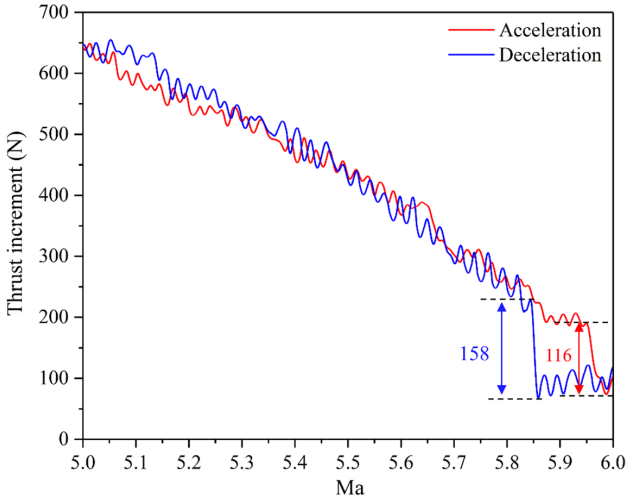

Fig. 12 Thrust increment vs Mach number of tests A1 and A3.

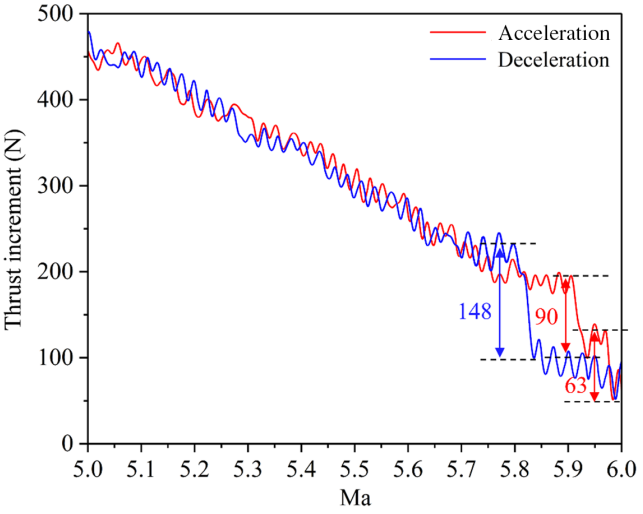

Fig. 14 Thrust increment vs Mach number of tests A2 and A4.

eration process, whereas the thrust burst can be shifted to Mach 5.85 during the deceleration process. In addition, the thrust amplitude of the abrupt change is 158 N in the deceleration process, which is greater than the related value of 116 N in the acceleration process. The differences in the characteristics of the abrupt phenomenon are induced by the hysteresis in combustion efficiency. Compared to the jet-wake flame stabilization mode, the combustion efficiency of cavity sheer-layer flame stabilization is much lower [34]. Therefore, during the deceleration process, a higher equivalence ratio and a lower Mach number are required to produce sufficient heat to make the flame stabilization mode transition happen compared to the acceleration process. Besides, considering the small difference in the variation range of the equivalence ratio between tests A1 and A3, the corresponding relationship between the experimental thrust increment and the equivalence ratio of the two tests is shown in Fig. 13. It can be seen that the equivalence ratio of the hysteresis loop is 0.03, which is much greater than the small difference between the equivalence ratio variation ranges of tests A1 and A3 shown in Table 3. That is to say, such a difference is not the main cause of the hysteresis mentioned before.

Furthermore, the effect of the variation-path changing of the incoming Mach number is not limited to the magnitude of the abrupt change in thrust and the corresponding Mach number. As shown in Fig. 14, only one abrupt change in the thrust with 148 N occurs in deceleration test A4, whereas two abrupt changes in the thrust with 90 N and 63 N are found in the corresponding acceleration test A2 with the same equivalence ratio variation. Due to the hysteresis in combustion efficiency, the Mach number observed while the abrupt change occurs in the deceleration test is lower than the corresponding value in the acceleration test, which is in agreement with Fig. 12. According to the preceding discussions, the times of the abrupt changes in the thrust are decided by the times of the flame stabilization mode transition during the test. In other words, the different variation paths of the incoming flow can even change the times of the flame stabilization mode transition. In summary, the variation in incoming flow conditions and adjustment in equivalence ratio will be seen to jointly determine the timing, characteristics, and process of flame stabilization mode transition.

In tests A3 and A4, there is only one abrupt change in thrust during the deceleration process. To better verify whether there would be two flame stabilization mode transitions during the deceleration process, test A5 is designed to continue to reduce the rate of change of the equivalence ratio on the basis of test A4. The conditions of test A5 are shown in Table 3.

The equivalence ratio of test A5 was basically unchanged throughout the experiment, so it can be considered that the effect of the equivalence ratio on combustion is relatively small, and the change of combustion in the combustor is mainly caused by the change of Mach number. It can be seen from Fig. 15 that two abrupt changes in thrust occurred during the experiment. This shows that by sustaining the equivalence ratio, two abrupt changes in thrust can also occur during the process of deceleration. The first abrupt change in thrust occurred at 16.2 s, the second one occurred at 17.0 s, and the time interval between the two abrupt changes in thrust was 0.8 s. To better understand the transition process of the flame stabilization mode in the combustor during the abrupt change in thrust, the pressure in the combustor is analyzed next. Figure 16 shows the pressure of the measuring point in the cavity. It can be seen that there are also two abrupt changes in the pressure in the combustor. Combined with the preceding analysis, it can be judged that there are two flame stabilization mode transitions in the combustor. First, the pressure at the trailing edge of the cavity increases, which indicates that the flame stabilization mode in the combustor is transitioned from the cavity shear-layer stabilized flame to the combined cavity shear-layer/recirculation stabilized flame. During the second abrupt change in the pressure process, the pressure of the three measuring points increased abruptly at the same time, which indicated that the flame stabilization mode in the combustor was transitioned from the combined cavity shear-layer/recirculation stabilized flame to the jet-wake stabilized flame at this time. The results of test A5 show that keeping the equivalence ratio unchanged, through changing the inflow conditions, can also make the transition of the flame stabilization mode in the combustor. Therefore, even under the condition of reducing the Mach number, which is not conducive to the occurrence of two abrupt changes in thrust, two abrupt changes in thrust still occur, whereas the equivalence ratio remains unchanged.

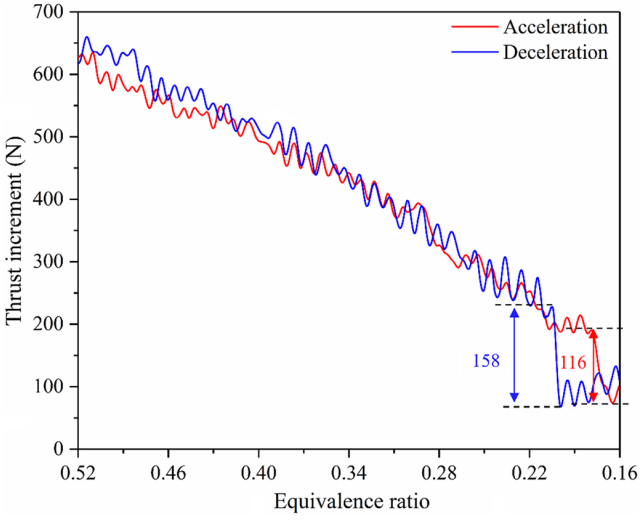

Fig. 13 Thrust increment vs equivalence ratio of tests A1 and A3.

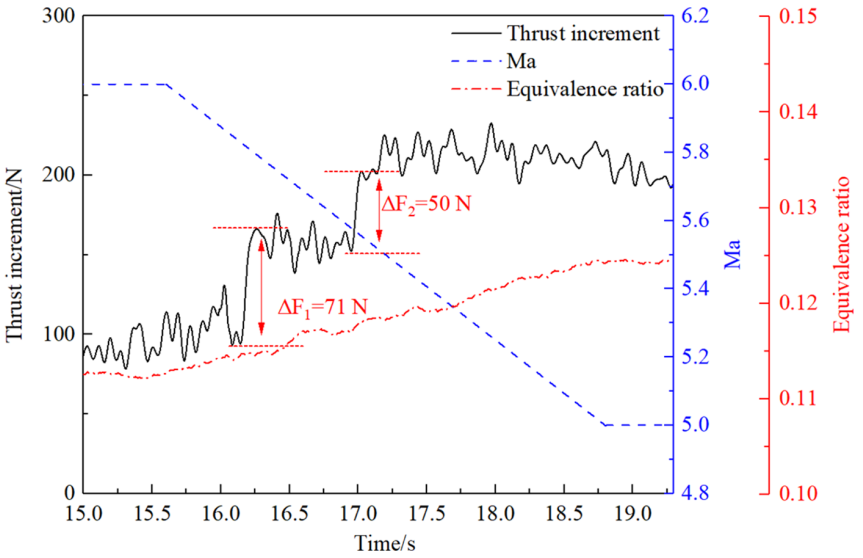

Fig. 15 Thrust increment and equivalence ratio vs time of test A5.

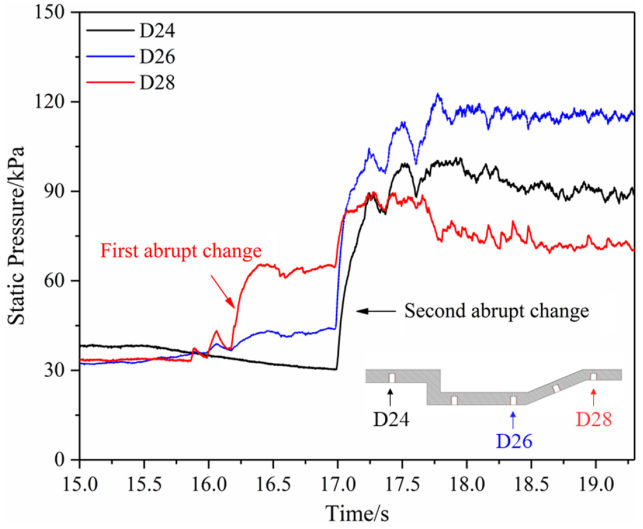

Fig. 16 Pressure of the measuring point near the cavity vs time of test A5.

IV. Conclusions

To enrich the understanding of the abrupt change phenomenon during the Mach number variation process, an experimental study was performed on a scramjet model with two rows of cavities under acceleration and deceleration operating conditions, namely, Mach number shifting between 5.0 and 6.0. Ethylene fuel was only injected immediately upstream of the back-row cavities to reduce variables. To better study the abrupt change in the thrust phenomenon, the experiments were designed as jet-wake stabilized combustion at a low Mach number and cavity shear-layer stabilized combustion at a high Mach number. In addition, different fuel supply strategies were carried out to make the flame stabilization mode transition happen. With the aid of the surface pressure measurement and the cassette strain gauge balance, the history of the surface pressure distribution and the thrust increment were recorded.

According to the currently obtained experimental results, an abrupt change at 116 N can be found in the history of the thrust increment of acceleration test A1 with the equivalence ratio varying from 0.53 to 0.16. Simultaneously, a relatively abrupt change was found in the pressure signals of the cavity pressure measuring points. Therefore, we can presume that the abrupt change in thrust is caused by the abrupt change in pressure. The abrupt change in pressure and thrust is the result of the flame stabilization mode varying from jet-wake stabilized combustion to cavity shear-layer stabilized combustion according to the pressure distribution characteristics of typical flame stabilization modes.

As the equivalence ratio varied from 0.30 to 0.15, two novel abrupt changes in the thrust occurred under the same acceleration condition as test A2. The target equivalence ratios of tests A1 and A2 are almost the same, but the initial equivalence ratio of test A1 is significantly higher than that of test A2. Due to the positive effect of the higher equivalent to the combustion intensity, the combustion flame mode transition timing is delayed by approximately 0.15 s in test A1 compared to test A2, and the transition Mach number increases from 5.90 to 5.96. Therefore, the differences in the incoming flow conditions and the fuel-supply status at the mode transition moment will directly affect the magnitude of the abrupt change in the pressure and thrust, and even the times of the abrupt changes.

Compared with the acceleration process, the abrupt change was accompanied by the flame stabilization mode transition in the deceleration process. However, due to the difference in the hysteresis in combustion efficiency, a higher equivalence ratio and a lower Mach number were required to produce sufficient heat to make the flame stabilization mode transition occur in the deceleration process compared to the acceleration process, because the magnitude of the abrupt change in thrust and the corresponding Mach number observed while the abrupt change emerges are different between the acceleration and deceleration tests. Furthermore, the different variation paths of the incoming flow can even change the times of the flame stabilization mode transition. By keeping the equivalence ratio basically unchanged during the deceleration process, there also will be two flame stabilization mode transitions during the deceleration process. In other words, the characteristics of the abrupt change during the flame stabilization mode transition process are determined by the combined effect of the changing paths of the incoming flow condition and the equivalence ratio.

Acknowledgment

This work was supported by the National Natural Science Foundation of China (grant nos. U2141220, 11902325, and 11672309).

References

[1] Huang, W., Liu, J., Yan, L., and Jin, L., "Multiobjective Design Optimization of the Performance for the Cavity Flameholder in Supersonic Flows," *Aerospace Science and Technology*, Vol. 30, No. 1, 2013, pp. 246–254. https://doi.org/10.1016/j.ast.2013.08.009

[2] Barnes, F. W., and Segal, C., "Cavity-Based Flameholding for Chemically-Reacting Supersonic Flows," *Progress in Aerospace Sciences*, Vol. 76, July 2015, pp. 24–41. https://doi.org/10.1016/j.paerosci.2015.04.002

[3] Hassanvand, A., Gerdroodbary, M. B., Fallah, K., and Moradi, R., "Effect of Dual Micro Fuel Jets on Mixing Performance of Hydrogen in Cavity Flameholder at Supersonic Flow," *International Journal of Hydrogen Energy*, Vol. 43, No. 20, 2018, pp. 9829–9837. https://doi.org/10.1016/j.ijhydene.2018.03.230

[4] Fallah, K., Gerdroodbary, M. B., Alinejad, J., and Ghaderi, A., "The Influence of Micro Air Jets on Mixing Augmentation of Fuel in Cavity Flameholder at Supersonic Flow," *Aerospace Science and Technology*, Vol. 76, May 2018, pp. 187–193. https://doi.org/10.1016/j.ast.2018.01.021

[5] Kobayashi, K., Tomioka, S., Kato, K., Murakami, A., and Kudo, K., "Performance of a Dual-Mode Combustor with Multistaged Fuel Injection," *Journal of Propulsion & Power*, Vol. 22, No. 3, 2006, pp. 518–526. https://doi.org/10.2514/1.19294

[6] Masumoto, R., Tomioka, S., Kudo, K., Murakami, A., Kato, K., and Yamasaki, H., "Experimental Study on Combustion Modes in a Supersonic Combustor," *Journal of Propulsion & Power*, Vol. 27, No. 2, 2011, pp. 346–355. https://doi.org/10.2514/1.B34020

[7] Gu, H. B., Li, Z., Li, F., Chen, L. H., Gu, S. L., and Chang, X. Y., "Characteristics of Supersonic Combustion with Hartmann-sprenger Tube Aided Fuel Injection," AIAA Paper 2011-2326, June 2012. https://doi.org/10.2514/6.2011-2326

[8] Noda, J., Ohkoshi, M., Kouchi, T., Masuya, G., Tomioka, S., Rockwall, R., and Goyne, C., "Quasi-One Dimensional Modeling on Vitiation Effects for a Dual-Mode Combustor," AIAA Paper 2012-5862, Sept. 2012. https://doi.org/10.2514/6.2012-5862

[9] Liu, C. Y., Yu, J. F., Wang, Z. G., Sun, M. B., Wang, H. B., and Grosshans, H., "Characteristics of Hydrogen Jet Combustion in a High-Enthalpy Supersonic Crossflow," *Physics of Fluids*, Vol. 31, No. 4, 2019, Paper 046105. https://doi.org/10.1063/1.5084751

[10] Cai, Z., Zhu, J. J., Sun, M. B., and Wang, Z. G., "Spark-Enhanced Ignition and Flame Stabilization in an Ethylene-Fueled Scramjet Combustor with a Rear-Wall-Expansion Geometry," *Experimental Thermal and Fluid Science*, Vol. 92, April 2018, pp. 306–313. https://doi.org/10.1016/j.expthermflusci.2017.12.007

[11] Feng, R., Huang, Y. H., Zhu, J. J., Wang, Z. G., Sun, M. B., and Wang, H. B., "Ignition and Combustion Enhancement in a Cavity-Based Supersonic Combustor by a Multi-Channel Gliding Arc Plasma," *Experimental Thermal and Fluid Science*, Vol. 120, Jan. 2020. https://doi.org/10.1016/j.expthermflusci.2020.110248

[12] Micka, D. J., and Driscoll, J. F., "Combustion Characteristics of a Dual-Mode Scramjet Combustor with Cavity Flameholder," *Proceedings of the Combustion Institute*, Vol. 32, No. 2, 2009, pp. 2397–2404. https://doi.org/10.1016/j.proci.2008.06.192

[13] Fotia, M. L., and Driscoll, J. F., "Ram-Scram Transition and Flame/Shock-Train Interactions in a Model Scramjet Experiment," *Journal of Propulsion & Power*, Vol. 29, No. 1, 2013, pp. 261–273. https://doi.org/10.2514/1.B34486

[14] Rasmussen, C. C., Driscoll, J. F., Hsu, K. Y., Donbar, J. M., Gruber, M. R., and Carter, C. D., "Stability Limits of Cavity-Stabilized Flames in Supersonic Flow," *International Symposium on Combustion*, Chicago, IL, 2004, pp. 2825–2834. https://doi.org/10.1016/j.proci.2004.08.185

[15] Rasmussen, C. C., Dhanuka, S. K., and Driscoll, J. F., "Visualization of Flameholding Mechanisms in a Supersonic Combustor Using PLIF," *Proceedings of the Combustion Institute*, Vol. 31, No. 2, 2007, pp. 2505–2512. https://doi.org/10.1016/j.proci.2006.08.007

[16] Rasmussen, C. C., Driscoll, J. F., Carter, C. D., and Hsu, K. Y., "Characteristics of Cavity-Stabilized Flames in a Supersonic Flow," *Journal of Propulsion & Power*, Vol. 21, No. 4, 2005, pp. 765–768. https://doi.org/10.2514/1.15095

[17] Sun, M. B., Wu, H. Y., Fan, Z. Q., Wang, H. B., Bai, X. S., Wang, G. Z., Liang, J. H., and Liu, W. D., "Flame Stabilization in a Supersonic Combustor with Hydrogen Injection Upstream of Cavity Flame Holders: Experiments and Simulations," *Proceedings of the Institution of Mechanical Engineers, Part G: Journal of Aerospace Engineering*, Vol. 225, No. 12, 2011, pp. 1351–1365. https://doi.org/10.1177/0954410011401498

[18] Wang, H. B., Wang, Z. G., and Sun, M. B., "Experimental Study of Oscillations in a Scramjet Combustor with Cavity Flameholders," *Experimental Thermal and Fluid Science*, Vol. 45, Feb. 2013, pp. 259–263. https://doi.org/10.1016/j.expthermflusci.2012.10.013

[19] Wang, H. B., Wang, Z. G., Sun, M. B., and Qin, N., "Combustion Characteristics in a Supersonic Combustor with Hydrogen Injection Upstream of Cavity Flameholder," *Proceedings of the Combustion Institute*, Vol. 34, No. 2, 2013, pp. 2073–2082. https://doi.org/10.1016/j.proci.2012.06.049

[20] Wang, H. B., Wang, Z. G., Sun, M. B., and Wu, H. Y., "Combustion Modes of Hydrogen Jet Combustion in a Cavity-Based Supersonic Combustor," *International Journal of Hydrogen Energy*, Vol. 38, No. 27, 2013, pp. 12078–12089. https://doi.org/10.1016/j.ijhydene.2013.06.132

[21] Yuan, Y. M., Zhang, T. C., Yao, W., Fan, X. J., and Zhang, P., "Characterization of Flame Stabilization Modes in an Ethylene-Fueled Supersonic Combustor Using Time-Resolved CH* Chemiluminescence," *Proceedings of the Combustion Institute*, Vol. 36, No. 2, 2017, pp. 2919–2925. https://doi.org/10.1016/j.proci.2016.07.040

[22] Yang, Q. C., Bao, W., Zong, Y. H., Chang, J. T., Hu, J. C., and Wu, M., "Combustion Characteristics of a Dual-Mode Scramjet Injecting Liquid Kerosene by Multiple Struts," *Proceedings of the Institution of Mechanical Engineers*, Vol. 229, No. 6, 2015, pp. 983–992. https://doi.org/10.1177/0954410014542447

[23] Yuan, Y. M., Zhang, T. C., Yao, W., and Fan, X. J., "Study on Flame Stabilization in a Dual-Mode Combustor Using Optical Measurements," *Journal of Propulsion and Power*, Vol. 31, No. 6, 2015, pp. 1524–1531. https://doi.org/10.2514/1.B35689

[24] Fotia, M. L., "Mechanics of Combustion Mode Transition in a Direct-Connect Ramjet–Scramjet Experiment," *Journal of Propulsion and Power*, Vol. 31, No. 1, 2015, pp. 69–78. https://doi.org/10.2514/1.B35171

[25] Xiao, B. G., Xing, J. W., Tian, Y., and Wang, X. Y., "Experimental and Numerical Investigations of Combustion Mode Transition in a Direct-Connect Scramjet Combustor," *Aerospace Science and Technology*, Vol. 46, Oct.–Nov. 2015, pp. 331–338. https://doi.org/10.1016/j.ast.2015.08.001

[26] Zhang, C. L., Chang, J. T., Feng, S., Ma, J. C., Zhang, J. L., and Bao, W., "Pressure Rising Slope Variation Accompanying with Combustion Mode Transition in a Dual-Mode Combustor," *Aerospace Science and Technology*, Vol. 68, Sept. 2017, pp. 370–379. https://doi.org/10.1016/j.ast.2017.05.034

[27] Zhang, C. L., Chang, J. T., Zhang, J. L., Bao, W., and Yu, D., "Effect of Continuous Mach Number Variation of Incoming Flow on Ram-Scram Transition in a Dual-Mode Combustor," *Aerospace Science and Technology*, Vol. 76, May 2018, pp. 433–441. https://doi.org/10.1016/j.ast.2018.02.027

[28] Kouchi, T., Masuya, G., Mitani, T., and Tomioka, S., "Mechanism and Control of Combustion-Mode Transition in a Scramjet Engine," *Journal of Propulsion and Power*, Vol. 28, No. 1, 2012, pp. 106–112. https://doi.org/10.2514/1.B34172

[29] Turner, J. C., and Smart, M. K., "Mode Change Characteristics of a Three-Dimensional Scramjet at Mach 8," *Journal of Propulsion and Power*, Vol. 29, No. 4, 2013, pp. 982–990. https://doi.org/10.2514/1.B34569

[30] Zhang, X., Yue, L. J., Huang, T. L., Zhang, Q. F., and Zhang, X. Y., "Numerical Investigation of Mode Transition and Hysteresis in a Cavity-Based Dual-Mode Scramjet Combustor," *Aerospace Science and Technology*, Vol. 94, Nov. 2019, pp. 1–10. https://doi.org/10.1016/j.ast.2019.105420

[31] Zhang, X., Zhang, Q. F., Wu, Z. J., Yue, L. J., Gao, Z. B., Luo, W. H., and Chen, H., "Experimental Study of Hysteresis and Catastrophe in a Cavity-Based Scramjet Combustor," *Chinese Journal of Aeronautics* (to be published). https://doi.org/10.1016/j.cja.2021.08.008

[32] Ikawa, H., "Rapid Methodology for Design and Performance Prediction of Integrated Supersonic Combustion Ramjet Engine," *Journal of Propulsion and Power*, Vol. 7, No. 3, 1991, pp. 437–444. https://doi.org/10.2514/3.23345

[33] Tian, L., Chen, L., Chen, Q., Li, F., and Chang, X. Y., "Quasi-One-Dimensional Multimodes Analysis for Dual-Mode Scramjet," *Journal of Propulsion and Power*, Vol. 30, No. 6, 2014, pp. 1559–1567. https://doi.org/10.2514/1.B35177

[34] Cao, D. G., Brod, H. E., Yokev, N., and Michaels, D., "Flame Stabilization and Local Combustion Modes in a Cavity-Based Scramjet Using Different Fuel Injection Schemes," *Combustion and Flame*, Vol. 233, 2021, Paper 111562. https://doi.org/10.1016/j.combustflame.2021.111562

R. D. Bowersox
Associate Editor